Organic Solar Cells Toward the Fabrication Under Air Environment

Victor Samuel Balderrama, Fernando Ávila-Herrera, José Guadalupe Sánchez, Josep Pallarès, *Senior Member, IEEE*, Osvaldo Vigil-Galán, Lluis F. Marsal, *Senior Member, IEEE*, and Magali Estrada, *Senior Member, IEEE*

***Abstract*—In this work, we analyze the performance parameters of the inverted organic solar cells (OSC) partially fabricated under an air environment, comparing them with those of similar solar cells manufactured totally under a nitrogen environment. Both solar cells use PTB7 and $PC_{70}BM$ as the active blend layer. The electrical parameters were extracted from the current density–voltage characteristic (*J–V*) under light and dark conditions. At the beginning, the OSCs partially fabricated under an air environment showed a similar performance as those manufactured under an N_2 environment. After 120 h, the power conversion efficiency of the OSCs partially fabricated under an air environment decreased 32% with respect to its initial value. The degradation process under the ISOS-D1 protocols was also analyzed.**

***Index Terms*—Air environment, incident photon-to-current efficiency (IPCE), ISOS-D1 protocols, performance parameters.**

I. Introduction

In recent years, the power conversion efficiency (*PCE*) in organic solar cells (OSCs) has been increased up to 11.5% [1]. Achievements such as semitransparency, flexibility, and light weight of component materials, as well as improved properties of organic semiconductor materials maintaining low-cost and low fabrication temperatures, have helped in the progress of this research on the bulk heterojunction (BHJ) OSC [2]–[5].

For large-scale fabrication, most reports agree that the roll-to-roll process seems to be the most promising one. However, this fabrication process is difficult to realize completely under a nitrogen environment, and it is well known that OSCs under an air environment degrade due to the low stability of some organic semiconductors when exposed under H_2O and O_2 environments.

Manuscript received August 31, 2015; revised November 17, 2015; accepted December 20, 2015. Date of publication January 19, 2016; date of current version February 18, 2016. This work was supported by the Consejo Nacional de Ciencia y Tecnología (CONACYT) under Project 237213 in Mexico and the National Postdoctoral Fellowship from CONACYT of the Call 2015-1 under Covenant 290941 and adjudged to the CVU No. 227699 in Mexico. This work was also supported by the Spanish Ministry of Economy and Competitiveness (MINECO) under Grant TEC2012-34397, the Catalan Government under Grant 2014-SGR-1344, and the ICREA under the ICREA Academia Award. The work of O. Vigil-Galán was supported by COFAA and EDI of IPN.

V. S. Balderrama, F. Ávila-Herrera, and M. Estrada are with the Sección de Electrónica del Estado Sólido, Departamento de Ingeniería Eléctrica, CINVESTAV, 07360 Ciudad de México, Mexico (e-mail: vbalderrama@cinvestav.mx; favila@cinvestav.mx; mestrada@cinvestav.mx).

J. G. Sánchez, J. Pallarès, and L. F. Marsal are with the Departament d'Enginyeria Electronica Electrica i Automatica, Rovira i Virgili University, 43007 Tarragona, Spain (e-mail: joseguadalupe.sanchez@urv.cat; josep.pallares@urv.cat; lluis.marsal@urv.cat).

O. Vigil-Galán is with the Escuela Superior de Física y Matemáticas del IPN, 07738 Ciudad de México, Mexico (e-mail: osvaldo@esfm.ipn.mx).

Color versions of one or more of the figures in this paper are available online at http://ieeexplore.ieee.org.

Digital Object Identifier 10.1109/JPHOTOV.2016.2514743

OSCs using tandem structures in combination with organic materials (i.e., P3HT:PCBM, MH301:PCBM, MH306:PCBM, etc.) have been manufactured by the roll-to-roll process [6]–[9].

However, up to now, the effects of exposing the samples to an air environment during the fabrication process are not well studied, because a more detailed analysis is necessary to indicate if this is possible and at which steps the effects are less important. Results regarding the performance parameters of OSCs with organic semiconductors of low band gap used under these conditions are not well known yet.

In this work, we report the analysis of the performance for two groups of inverted OSCs: one fabricated totally under nitrogen ambient and the other exposed to air environment during its processing. The device structure had the next stack: indium tin oxide (ITO)/poly[(9,9-bis(3-(N,N-dimethylamino)propyl)-2,7-fluorene)-alt-2,7-(9,9–dioctylfluorene)] (PFN)/poly[[4,8-bis[(2-ethylhexyl)-oxy]benzo[1,2-b:4,5-b']dithiophene-2,6-diyl][3-fluoro-2-[(2-ethylhexyl) carbonyl]thieno[3,4-b]thiophenediyl]] (PTB7): [6,6]-phenyl-C_{71}-butyric acid methyl ($PC_{70}BM$)/vanadium oxide (V_2O_5)/silver (Ag). The PFN and the PTB7:$PC_{70}BM$ layers were prepared and deposited under a nitrogen environment. A group of samples were taken out of the glove box and exposed under an air environment for 10 min before depositing by thermal evaporation the V_2O_5 and Ag layers. A second group of samples were fabricated completely under an N_2 environment for comparison with samples from the first group. Current density–voltage (*J–V*) characteristics were measured for both groups of inverted OSC samples under dark and light conditions to extract the basic parameters and relate them to the physical mechanisms present. Optical properties such as incident photon-to-current efficiency (IPCE) and absorbance coefficient were obtained from the photovoltaic devices to understand the differences between the two groups of cells, as well as factors that limit the *PCE*. The knowledge of this behavior is important for the design, fabrication, and optimization of the OSC and to reduce the effects of manufacturing under air conditions during industrial process development in the transition from the laboratory to the large-scale fabrication conditions.

II. Experimental Details

A. Materials

ITO-coated glass substrates were purchased from PsiOTec Ltd. PTB7, and PFN materials were purchased from One-material Company with $M_w \sim 128\,\text{kg} \cdot \text{mol}^{-1}$ and $M_w \sim 44.5\,\text{kg} \cdot \text{mol}^{-1}$, respectively. $PC_{70}BM$ with $M_w \sim 1031.0\,\text{g} \cdot \text{mol}^{-1}$ was purchased from Solenne BV. High-purity (99.99%)

silver wire was obtained from Testbourne Ltd., and vanadium oxide was purchased from Sigma-Aldrich.

B. Device Fabrication

Two different groups of OSCs were manufactured under different environments. The first batch of cells was totally fabricated under an N_2 environment (A OSC-group). The second batch was partially manufactured under nitrogen and partially in air environment (B OSC-group). Both groups of inverted photovoltaic devices were fabricated on precleaned, patterned, ITO glass substrate (10 Ω/square). The PFN interlayer material was dissolved in methanol and mixed with a small amount of acetic acid (2 μl $\cdot$ mL^{-1}), and its solution (concentration, 2 mg $\cdot$ mL^{-1}) was spin-coated on top of the precleaned ITO substrate at 3500 r/min, obtaining a thickness of 10 nm. The PTB7:PC_{70}BM active blend with a weight ratio of 1 : 1.5 was dissolved in chlorobenzene (CB) and 1,8-diiodooctane (DIO) (CB:DIO = 97:3 by volume) to get 25 mg $\cdot$ mL^{-1} of the total solution and left stirring overnight. The blend solution was deposited on top of PFN layer by spin coating at 800 r/min for 30 s, obtaining the thickness of 100 nm. Until this processing step, both A and B groups of OSCs were fabricated under nitrogen conditions. Afterward, samples from B group were exposed under an air environment for 10 min at 23 °C and relative humidity (RH) of 33% under darkness, while group A of cells remained under an N_2 environment. Subsequently, the B group of films was exposed under vacuum conditions to make desorption of H_2O and O_2 for 3 h at 1.5 $\times$ 10^{-5} torr. Later, the anode layers, consisting of 5 nm of V_2O_5 and 100 nm of Ag, were deposited by thermal evaporation at 1.5 $\times$ 10^{-5} torr at a rate of 0.18 nm/s and 0.1–0.3 nm/s respectively, on top of the active layer, for both OSC groups. The active area for the devices was 0.09 cm^2 as defined by the geometric overlap between ITO and Ag layers. No further annealing of the OSC was done after the evaporation of metallic contacts. The devices were measured under a nitrogen environment.

C. Measurements

The absorption spectrum was measured at room temperature with a Jasco V-670 UV/VIS/NIR spectrophotometer. The *J–V* characteristics under light and dark of the devices were measured at room temperature using a Keithley 236 and Keithley 2420 source measurement unit in combination with a solar simulator (Oriel Corporation Sol1A class type ABB, Xenon arc lamp), automatically controlled with a computer. Appropriate filters were used to reproduce the AM 1.5G spectrum. A light intensity of 100 mW/cm^2 (1 sun) was applied to test the OSC devices under illumination. The light intensity was calibrated with a Solarex Corporation certified monocrystalline silicon photodiode. Film thicknesses were measured by a Gaertner Scientific L2W16S633 ellipsometer. The incident-photon-to-current efficiency of the devices was measured illuminating the device through the light source and monochromator, and the resulting current was measured using a Keithley 485 electrometer under short-circuit condition ($V = 0$ V).

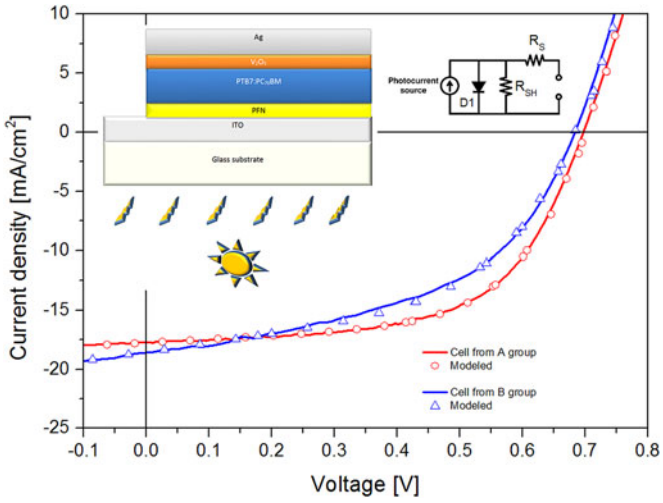

Fig. 1. Current–voltage (*J–V*) characteristics of PTB7:PC_{70}BM inverted OSCs from A and B groups under 100 mW/cm^2 equivalent illumination intensity corresponding to AM 1.5G sun light standard. (Inset) Device structure and the equivalent circuit used. Measured characteristics (solid lines) and modeled characteristics (open symbols).

D. Degradation Testing Conditions and Protocols

The stability testing for both groups of OSCs reported here was in accordance with ISOS-D1 protocols [10], [11]. The A and B groups of OSC remained in a dry N_2 environment (H_2O < 0.1 ppm, O_2 < 0.1 ppm) in the dark and at 23 °C during the experiment. OSCs were not encapsulated.

III. Results and Discussion

The analysis of the OSC was done in two parts. First, the performance parameter analysis was done just after sample fabrication; second, analysis of the performance parameters was done over time (degradation).

A. Just After Sample Fabrication

Fig. 1 shows the *J–V* characteristics of the inverted PTB7:PC_{70}BM solar cells of both groups A and B under illumination at 1 sun (100 mW/cm^2). Table I summarizes the average and best performance parameters (i.e., open-circuit voltage (V_{OC}), short-circuit current density (J_{SC}), fill factor (*FF*), and PCE) of the inverted OSCs (from 16 devices) after fabrication. Best results for each group of cells were analyzed.

Inverted OSC from A group totally manufactures under an N_2 environment and inverted OSC from B group partially manufactured under an air environment showed a *PCE* of 7.42% and 6.20%, respectively. The V_{OC}, *FF*, and *PCE* for the B OSC-group were 2.0%, 19.7%, and 16.4% less than that of the A OSC-group, respectively. On the other hand, the J_{SC} of B OSC-group was 5.0% higher than that of the A OSC-group.

The enhancement observed in the J_{SC} for the B OSC-group can be due to the increment of the polymer conductivity during the exposition of the samples for 10 min under air atmosphere before the deposition of the metallic contact. Some scientific reports have shown this effect on the polymeric materials [12],

TABLE I
PERFORMANCE PARAMETERS OF THE OSC THROUGH TIME

Group	Degradation time	V_{OC}^{a} Best-(Average) (mV)	J_{SC}^{b} Best-(Average) (mA cm^{-2})	FF^{c} Best-(Average) (%)	PCE^{d} Best-(Average) (%)	$R_{S0\text{-il}}^{e}$ ($\Omega \cdot$ cm^2)	$R_{SH0\text{-il}}^{f}$ (k$\Omega \cdot$ cm^2)	$R_{S0\text{-dk}}^{g}$ ($\Omega \cdot$ cm^2)	$R_{SH0\text{-dk}}^{h}$ (k$\Omega \cdot$ cm^2)
A	Fresh	698 (693 $\pm$ 4)	17.75 (17.43 $\pm$ 0.31)	61 (60 $\pm$ 1)	7.42 (7.30 $\pm$ 0.11)	1.96	0.36	4.91	135.90
	After 24 h	693	17.64	56	6.83	3.03	0.81	4.79	147.05
	After 120 h	670	16.91	60	6.84	2.64	0.68	4.90	124.66
B	Fresh	684 (680 $\pm$ 5)	18.60 (18.03 $\pm$ 0.51)	49 (48 $\pm$ 1)	6.20 (6.11 $\pm$ 0.17)	1.92	0.14	3.07	19.12
	After 24 h	678	17.25	45	5.26	5.17	0.12	6.93	2.12
	After 120 h	700	15.70	39	4.20	10.94	0.10	18.26	3.76

The A OSC-group was totally manufactured under nitrogen atmosphere. The B OSC-group was partially manufactured under an air environment. [a] Open-circuit voltage. [b] Short-circuit current. [c] Fill factor. [d] Power conversion efficiency. The applied equivalent illumination intensity was 100 mW/cm^2 after spectral mismatch correction using AM 1.5 G solar simulator. [e] Series resistance per unit area under illumination. [f] Shunt resistance per unit area under illumination. [g] Series resistance per unit area under dark. [h] Shunt resistance per unit area under dark.

[13], quantifying the doping concentration of the material reached after air exposition. PTB7:PC$_{70}$BM OSC manufactured under air atmosphere was reported in [14] and observed the increment on J_{SC}. In other studies when the RH is increased, J_{SC} also increased, as was reported in [15] and [16] and in the supplementary information of [17]. Similar effect was also observed in our devices partially fabricated under an air at 33% RH, just measured after the samples fabrication. Therefore, the increase in J_{SC} in our samples can be explained by the insertion of H_2O and O_2 in the active layer during the short time exposition under air. The absorptions of H_2O and O_2 combined with photon-induced chemical reactions during the measurements are some of the mechanisms for the chemical transformation of the molecules in the active layer, as reported in [18] and [19].

As a result of the chemical transformation taking place at the active layer when exposed to air, new trap states are expected to be created. In [20]–[22], the trap distribution of a P3HT:PCBM blend was studied by a fractional stimulated current technique. The authors observed two different trap states, with activation energies of 50 and 105 meV. They associated the first type of states to the intrinsic localized states of the polymer, while the other type varied with exposure conditions to oxygen. Although we have not found a similar study for the PTB7:PC$_{70}$BM blend, the effect related to the insertion of H_2O and O_2 molecules can take place in any polymer when exposed under air. However, it is not possible to distinguish the contribution of each of these factors on the overall performance of the device in this experiment.

The inset in Fig. 1 shows the electrical equivalent circuit used to describe dark and illuminated *J–V* characteristics, where D1 represents the PTB7:PC$_{70}$BM heterojunction. R_{SH} and R_S are shunt and series resistances associated with diode D1 and the overall cell structure. The *J–V* curve is expressed as usual [23]:

$$J = J_0 \left[\exp \frac{q*(V - J*A*Rs)}{nkT} - 1\right] + \frac{(V - J*A*Rs)}{R_{SH}} - J_{ph} \quad (1)$$

where J_0 is the saturation current density, A is the area of the cell, J_{ph} is the photocurrent, n is the ideality factor, k is the Boltzmann constant, and q is the elementary charge.

Fig. 2 shows the semi-log *J–V* characteristics under dark conditions for the two groups of OSCs. It is well known that R_S can be related to the resistance and thickness of the active layer, the contact resistance between the metal and active layer, the transport properties of the semiconductor material, and the type of the selective contacts used for the devices. Its value per unit area, i.e., R_{S0}, can be calculated by the inversed slope of the *J–V* curve at the highest operating voltage where the curve becomes linear: $R_{S0} = (J/V)^{-1}$, as has been reported [11], [23]. In this study, the series resistances $R_{S0\text{-il}}$ and $R_{S0\text{-dk}}$ were obtained from the measurement *J–V* characteristic modeled by (1) under illumination and darkness. The values for each group of OSC structure are shown in Table I. In general, $R_{S0\text{-il}}$ and $R_{S0\text{-dk}}$ for the B OSC-group presented values 2.0% and 37.4% lower than that for the A OSC-group just after fabrication, respectively. The decrease in the series resistances observed for the B OSC-group just after fabrication can be attributed to the increase of the active layer conductivity after the 10 min exposition under an air environment (H_2O and O_2).

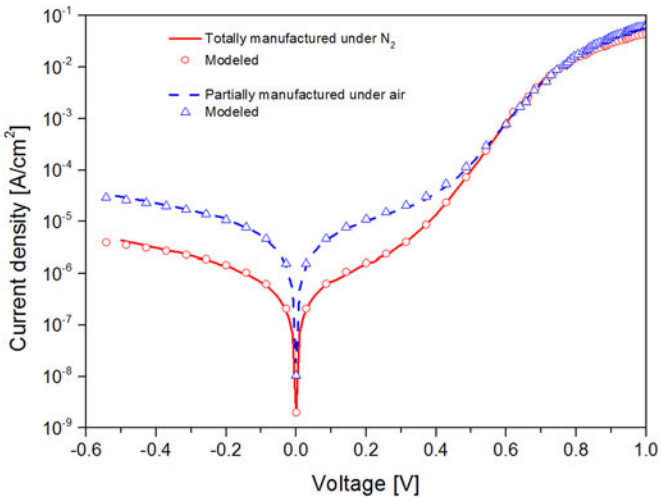

Fig. 2. Semi-log *J–V* curve under darkness for both groups of cells manufactured. Measured characteristics (solid lines) and modeled characteristics (open symbols).

The shunt resistance R_{SH} is related to the recombination of charge carriers near the dissociation site (e.g., the donor/acceptor interface of the BHJ) and depends on the transport properties of the semiconductor as well. The value of

TABLE II
IDEALITY FACTOR AND SATURATION CURRENT

Group of OSC and condition		n^a_{dk}	$J^b_{0\mathrm{dk}}$ (A · cm^{-2})
A	Fresh	1.75	1.33×10^{-9}
B	Fresh	1.95	6.06×10^{-9}

The A OSC-group was totally manufactured under nitrogen atmosphere. The B OSC-group was partially manufactured under an air environment. [a] Ideality factor under dark. [b] Saturation current for the diode under dark. All the parameters were extracted from the diode model [see (1)].

the shunt resistance per unit area, i.e., R_{SH0}, can be determined by calculating the inverse slope around 0 V of the *J–V* curve, $R_{\mathrm{SH0}} = (J/V)^{-1}$. When the cell is not illuminated, this parallel shunt resistance is expected to reflect the intrinsic conductivity of the materials. Under illumination, light-induced charge generation (photodoping) caused by the charge transfer between the donor and the acceptor is expected to reduce the shunt resistance dramatically, as was observed in our results [11], [23]. In this study, the shunt resistances $R_{\mathrm{SH0\text{-}il}}$ and $R_{\mathrm{SH0\text{-}dk}}$ were obtained from the *J–V* characteristic modeled by (1) under illumination and darkness, respectively, and their values are shown in Table I. Continuing with the analysis, in general, the $R_{\mathrm{SH0\text{-}il}}$ and $R_{\mathrm{SH0\text{-}dk}}$ on the B OSC-group were 2.6 times and 7.1 times lower, respectively, than those of the A OSC-group just after fabrication. The decrease in the shunt resistance presented on the B OSC-group just after fabrication can be attributed to the increase in the recombination of the charge carriers at the interface of the donor/acceptor of the BHJ compared with the A OSC-group.

It is well known that the ideality factor reflects the dominant transport mechanism in the diode. Table II shows the ideality factor extracted from the modeled *J–V* curve under darkness for the A and B OSC-groups, which were 1.75 and 1.95, respectively. The ideality factor near to 2 for the B OSC-group indicates that recombination is the predominant transport mechanism, while for the A OSC-group, a combination of diffusion with recombination mechanisms seems to be present.

The saturation current in OSC is associated with the number of charges capable of overcoming the energetic barrier in the reverse direction. It represents the minority charge density in the vicinity of the barrier. In this analysis, J_0 was extracted from the modeled *J–V* curve under darkness. The J_0 for the B OSC-group was 4.6 times higher than that for the A OSC-group. The higher the diode recombination, the greater J_0 will be [23]–[25]. Some reports claim that increasing of J_0 can be explained by increased doping or a source of additional minority carries created near the interface of the active layer [26]. In our case, the solar cells manufactured partially under an air environment presented higher J_0 and lower R_{SH}, where the recombination is the predominant transport mechanism as a result of incremented doping in the active layer.

B. Organic Solar Cell Degradation Over Time

In order to see the degradation behavior for both groups of OSCs, the ISOS-D1 protocols were applied.

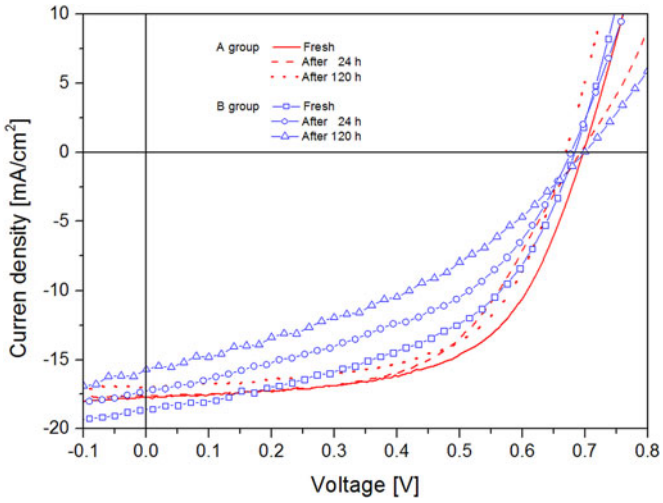

Fig. 3. Illuminated *J–V* curves of inverted PTB7:$PC_{70}BM$ solar cells for the A group (devices fabricated under an N_2 environment) and for the B group (devices partially fabricated under air) for different degradation times under a nitrogen environment during 120 h. All the devices were measured under AM 1.5G spectrum condition (100 mW/cm^2).

During the degradation analyses, both groups of OSC remained under a nitrogen environment. Fig. 3 shows typical degradation of *J–V* curves under illumination, for both OSC-groups kept in an N_2 environment. The samples were only exposed to light during the *J–V* measurement (for less than 1 min per measurement) and, afterward, were returned to the glove box for storage under darkness. Table I shows the performance parameters from fresh to 120 h under an N_2 environment for both OSC-groups.

According to ISOS-D1 protocols, the lifetime for *PCE* of samples exposed to nitrogen for the A and B OSC-groups at T_{S80} were $>$120 and 24 h, respectively. The performance parameters for the A OSC-group at 120 h such as V_{OC}, J_{SC}, *FF*, and *PCE* decreased slowly being 4%, 4.5%, 0%, and 7.8%, respectively. In the same period of time, for the B OSC-group, the performance parameters such as J_{SC}, *FF*, and *PCE* fell 21%, 22%, and 36%, while the V_{OC} increased in 2%. The quick fall of the performance parameters of the B group is due to the exposure to air environment (H_2O and O_2), where these molecules were absorbed by the active layer of the photovoltaic device. Some scientific reports point out that the main degradation through time for the P3HT:PCBM active layer expose under an air environment and storage in darkness is due to the water influence [17]. On the other hand, the PTB7 polymer can be degraded with facility in presence with an oxygen molecule, as reported in [19], but is more quickly in combination with the light [9], [18], [19], [27]. On the basis of the above, we suggest that the device B group degraded with more influence by O_2 molecules than by H_2O.

The decreased J_{SC} observed in the B OSC-group through time is due to doping and can be explained by an increased bimolecular recombination probability. Since doping implies additional charges within the device, it leads to less band bending and, therefore, a reduced electrical field within the solar cell. As a consequence, the extraction time for the charge carriers increases, leading to a higher recombination probability and, thus,

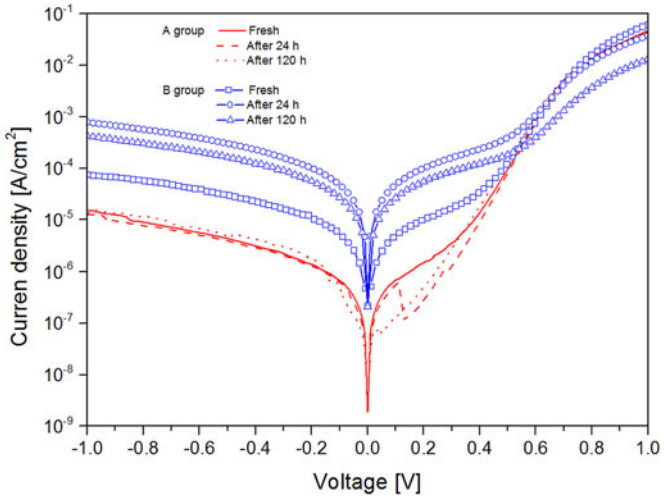

Fig. 4. Degradation with time of semi-log *J–V* curves under dark of inverted PTB7:PC_{70}BM solar cells for the A group (devices fabricated under an N_2 environment) and for the B group (devices partially fabricated under air). Samples were kept under a nitrogen environment between measurements.

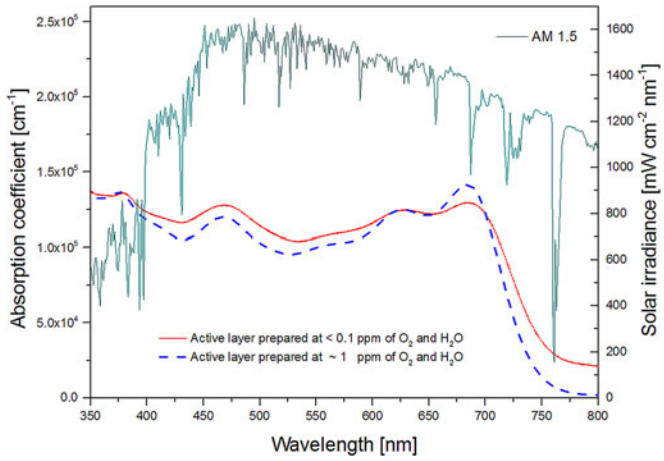

Fig. 5. Absorption coefficient of PTB7:PC_{70}BM blend layers manufactured under a nitrogen environment with H_2O and O_2 $<$ 0.1 ppm (red solid line) and H_2O and O_2 $\sim$ 1 ppm conditions (blue dashed line). The solar irradiance under AM 1.5 is shown in the same graph.

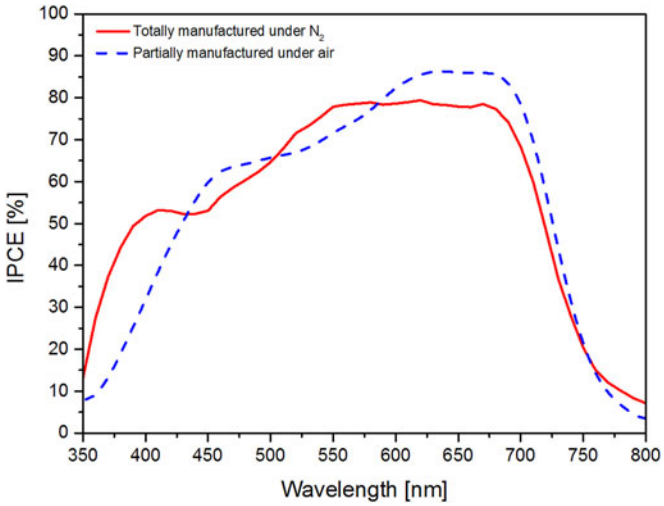

Fig. 6. IPCE spectrum of inverted OSCs from A group totally manufactured under N_2 and B group partially manufactured under air conditions. The IPCE was just measured after sample fabrication.

to a lower short circuit current over time. A similar behavior was reported in [22].

The loss of $J_{\rm SC}$ and *FF* and a small increase of $V_{\rm OC}$ in the B OSC-group over time are due to a decrease of the mobility on solar cell performance. Scientific reports point out that a lower mobility leads to a higher extraction time for the charge carriers and, therefore, to an enhanced bimolecular recombination probability, which results in the decreased *FF*. Therefore, the *FF* results obtained from *J–V* characteristics under light over time of B OSC-group presented this same behavior, which are strongly supported by the reports in [22]. At the same time, the charge extraction becomes less efficient. The slightly increasing open-circuit voltage is due to a lower Langevin recombination rate due to decreased mobilities. The higher charge carrier densities and their more balanced distribution reduce the internal electric field and, therefore, increase the open-circuit voltage [22], [28].

Fig. 4 shows semi-log *J–V* curves under dark for both OSC-groups kept in an N_2 environment. The R_{S0} and $R_{\rm SH0}$ were extracted from the *J–V* characteristic modeled by (1), and the parameters are shown in Table I. The small increase of R_{S0} for the A OSC-group can be attributed to a slow degradation mechanism resulted from the chemical reaction between the polymeric and metallic materials and not to the effect of very low content of both H_2O and O_2 in the N_2 gas ($<$0.1 ppm). Similar behavior was reported for PTB1:PCBM OSC in [11].

However, the $R_{S0\text{-dk}}$ for the B OSC-group increased six times more rapidly. This increase is expected to be mainly due to the reaction of H_2O or O_2 with the blend layer. These molecules diffused into the blend layer when the samples were exposed under an air environment during the manufacture of the photovoltaic devices.

The $R_{\rm SH0\text{-dk}}$ for the A OSC-group remains quite stable and is on the order 10^5 Ω, whereas the B OSC-group is on the order 10^4 Ω.

Fig. 5 shows the absorption coefficient for the pristine PTB7:PC_{70}BM films. The films were manufactured under two nitrogen environment conditions variating the ppm of H_2O and O_2. The first and second films were manufactured at $<$0.1 ppm of H_2O and O_2 and $\sim$1 ppm of H_2O and O_2, respectively.

From the absorption coefficient, we can see that the absorbance of PTB7:PC_{70}BM film manufactured at $<$0.1 ppm of H_2O and O_2 is similar to that reported in [13], [18], [19], [29], and [30]. The absorption coefficient from 350 to 625 nm was major for the sample manufactured under a nitrogen atmosphere. While the samples were exposed to 1 ppm of H_2O and O_2, the absorption coefficient maximum is slightly less in the same range of wavelength. The peak centered at 685 nm for the film fabricated at $\sim$1 ppm of H_2O and O_2 was 10% higher than that for that fabricated at $<$0.1 ppm condition. The absorption coefficient increment at 685 nm can be due to the introduction by H_2O and O_2 into the active layer. In the same Fig. 5, the solar irradiance is also shown to see where the active layer absorbs more photons.

Fig. 6 compares the IPCE spectra for the devices totally manufactured under nitrogen and partially under an air environment. IPCE for the A OSC-group is similar to the absorption coefficient spectrum throughout the range from 400 and 700 nm reported in [29].

The IPCE for the A and B OSC-groups between 550–700 and 625–700 nm was around of 79% and 86%, respectively. Short-circuit current density was obtained by integrating under the IPCE curve. The short-circuit current density for the A and B OSC-groups were of 17.6 and 18.5 mA/cm^2, respectively, which strongly support the values obtained from the *J–V* characteristics under light, as seen above. The shoulder observed at 400 nm for the devices totally fabricated under nitrogen atmosphere was up-shift to 465 nm for samples partially manufactured under an air atmosphere. The up-shift of the shoulder can be due to the changes of the OSC active film due to the influence of H_2O and O_2, which modified the optical properties.

The difference observed between the IPCE in short-wavelength region of the devices fabricated under a nitrogen and partially air environment is due to the degradation of the constituents of the active layer (PTB7 and $PC_{70}BM$).

In [27], it was reported that PTB7 chains can be modified by photooxidation, even in inert conditions. In this case, it is considered that the exposure to light can separate oxygen atoms from the polymer chain, creating new species. Knowing this effect, it is possible to assume that when exposure to ambient conditions, the effect of oxygen may also create new species and be predominant in the degradation of the PTB7 polymer.

In [19], the authors applied Raman spectroscopy to monitor molecular level changes in PTB7:$PC_{70}BM$ blends after photodegradation, observing also the formation of new species, in this case hydroxyl formation.

For the PCBM fullerene, the degradation by water molecule is predominant, as was reported in [31]. The intensities obtained from the absorption coefficient spectra and from EQE are well correlated in this analysis, observing a reduction of the absorption coefficient spectrum, as well as a reduction in the charge collection for EQE spectrum on the same range of wavelength. Similar behavior was observed on P3HT:PCBM devices reported by Guerrero *et al.* [32].

Other effects that were also considered are the reflections of all the layers from the photovoltaic cell, because they played an important role and modified the optical properties in it.

IV. Conclusion

The effect of exposing inverted OSC using PTB7:$PC_{70}BM$ as the active layer to ambient conditions for 10 min, during its manufacturing process, was analyzed. Just after fabrication, B OSC-group showed the same $V_{\rm OC}$, 5% higher $J_{\rm SC}$, and 2% smaller $R_{S0\text{-il}}$ than that for the A OSC-group totally manufactured under an N_2 environment. The increase of the $J_{\rm SC}$ and reduction of R_S is due to the increment on conductivity of the active blend layer when the samples were exposed for 10 min under air environment before the metal contact deposition. For the OSC after 24 h of degradation, the *FF* and *PCE* reduced around 8% and 15%, respectively, while $R_{{\rm SH}0-il}$ decreased around 14%, and after 120 h, the degradation was more significant compared with A OSC-group. The lifetime (T_{S80}) for the device B OSC-group was 24 h compared with >120 h for the A OSC-group. Results indicate that it seems possible to reduce some of the strict rules in the fabrication of OSCs under an N_2 environment, in order to fabricate OSC under an air environment for an acceptable transition from laboratory to large scale and reduce cost production.

References

[1] M. A. Green, K. Emery, Y. Hishikawa, W. Warta, and E. D. Dunlop, "Solar cell efficiency tables (Version 45)," *Prog. Photovoltaics Res. Appl.*, vol. 23, pp. 1–9, 2015.

[2] C. J. Brabec, "Organic photovoltaics: Technology and market," *Sol. Energ. Mater. Sol. Cells*, vol. 83, pp. 273–292, 2004.

[3] V. S. Balderrama *et al.*, "Correlation between P3HT inter-chain structure and Jsc of P3HT:PC[70]BM blends for solar cells," *Microelectron. Rel.*, vol. 53, pp. 560–564, 2013.

[4] P. Reiss, E. Couderc, J. De Girolamo, and A. Pron, "Conjugated polymers/semiconductor nanocrystals hybrid materials-preparation, electrical transport properties and applications," *Nanoscale*, vol. 3, pp. 446–489, 2011.

[5] Y. Q. Wong, H. Y. Wong, C. S. Tan, and H. F. Meng, "Performance optimization of organic solar cells," *IEEE Photon. J.*, vol. 6, no. 4, pp. 1–26, Aug. 2014.

[6] T. R. Andersen *et al.*, "Scalable, ambient atmosphere roll-to-roll manufacture of encapsulated large area, flexible organic tandem solar cell modules," *Energy Environ. Sci.*, vol. 7, pp. 2925–2933, 2014.

[7] M. Jørgensen *et al.*, "Stability of polymer solar cells," *Adv. Mater.*, vol. 24, pp. 580–612, 2012.

[8] R. R. Søndergaard, M. Hösel, and F. C. Krebs, "Roll-to-roll fabrication of large area functional organic materials," *J. Polym. Sci. B, Polym. Phys.*, vol. 51, pp. 16–34, 2013.

[9] F. C. Krebs, S. A. Gevorgyan, and J. Alstrup, "A roll-to-roll process to flexible polymer solar cells: Model studies, manufacture and operational stability studies," *J. Mater. Chem.*, vol. 19, pp. 5442–5451, 2009.

[10] M. O. Reese *et al.*, "Consensus stability testing protocols for organic photovoltaic materials and devices," *Sol. Energ. Mater. Sol. Cells*, vol. 95, pp. 1253–1267, 2011.

[11] V. S. Balderrama *et al.*, "Degradation of electrical properties of PTB1:PCBM solar cells under different environments," *Sol. Energy Mater. Sol. Cells*, vol. 125, pp. 155–163, 2014.

[12] I. Mejia, M. Estrada, A. Cerdeira, and B. Iniguez, "Reversible electrical characteristics in PMMA on P3HT OTFTs," *ECS Trans.*, vol. 9, pp. 383–388, 2007.

[13] V. S. Balderrama *et al.*, "Relation of polymer degradation in air with the charge carrier concentration in PTB1, PTB7, and PCBM layers used in high-efficiency solar cells," *IEEE J. Photovoltaics*, vol. 5, no. 4, pp. 1093–1099, Jul. 2015.

[14] E. A. A. Arbab, B. Taleatu, and G. T. Mola, "Environmental stability of PTB7:PCBM bulk heterojunction solar cell," *J. Mod. Opt.*, vol. 61, pp. 1749–1753, 2014.

[15] M. Lira-Cantu and F. C. Krebs, "Hybrid solar cells based on MEH-PPV and thin film semiconductor oxides (TiO_2, Nb_2O_5, ZnO, CeO_2 and CeO_2–TiO_2): Performance improvement during long-time irradiation," *Sol. Energy Mater. Sol. Cells*, vol. 90, pp. 2076–2086, 2006.

[16] M. Lira-Cantu, K. Norrman, J. W. Andreasen, N. Casan-Pastor, and F. C. Krebs, "Detrimental effect of inert atmospheres on hybrid solar cells based on semiconductor oxides," *J. Electrochem. Soc.*, vol. 154, pp. B508–B513, 2007.

[17] K. Norrman, M. V. Madsen, S. A. Gevorgyan, and F. C. Krebs, "Degradation patterns in water and oxygen of an inverted polymer solar cell," *J. Amer. Chem. Soc.*, vol. 132, pp. 16883–16892, 2010.

[18] Y. W. Soon *et al.*, "Correlating triplet yield, singlet oxygen generation and photochemical stability in polymer/fullerene blend films," *Chem. Commun.*, vol. 49, pp. 1291–1293, 2013.

[19] J. Razzell-Hollis *et al.*, "Photochemical stability of high efficiency PTB7:PC70BM solar cell blends," *J. Mater. Chem. A*, vol. 2, pp. 20189–20195, 2014.

[20] J. Schafferhans, A. Baumann, C. Deibel, and V. Dyakonov, "Trap distribution and the impact of oxygen-induced traps on the charge transport in poly(3-hexylthiophene)," *J. Appl. Phys.*, vol. 93, p. 093303, 2008.

[21] C. R. McNeill and N. C. Greenham, "Charge transport dynamics of polymer solar cells under operating conditions: Influence of trap filling," *J. Appl. Phys.*, vol. 93, p. 203310, 2008.
[22] J. Schafferhans, A. Baumann, A. Wagenpfahl, C. Deibel, and V. Dyakonov, "Oxygen doping of P3HT:PCBM blends: Influence on trap states, charge carrier mobility and solar cell performance," *Org. Electron.*, vol. 11, pp. 1693–1700, 2010.
[23] C. Waldauf, M. C. Scharber, P. Schilinsky, J. A. Hauch, and C. J. Brabec, "Physics of organic bulk heterojunction devices for photovoltaic applications," *J. Appl. Phys.*, vol. 99, p. 104503, 2006.
[24] A. Cheknane, H. S. Hilal, F. Djeffal, B. Benyoucef, and J.-P. Charles, "An equivalent circuit approach to organic solar cell modelling," *Microelectron. J.*, vol. 39, pp. 1173–1180, 2008.
[25] V. S. Balderrama *et al.*, "Influence of P3HT:PCBM blend preparation on the active layer morphology and cell degradation," *Microelectron. Rel.*, vol. 51, pp. 597–601, 2011.
[26] A. Kumar *et al.*, "Origin of radiation-induced degradation in polymer solar cells," *Adv. Funct. Mater.*, vol. 20, pp. 2729–2736, 2010.
[27] S. Shah and R. Biswas, "Atomic pathways underlying light-induced changes in organic solar cell materials," *J. Phys. Chem. C*, vol. 119, pp. 20265–20271, Sep. 3, 2015.
[28] D. Cheyns *et al.*, "Analytical model for the open-circuit voltage and its associated resistance in organic planar heterojunction solar cells," *Phys. Rev. B*, vol. 77, p. 165332, 2008.
[29] L. Leonat *et al.*, "4% Efficient polymer solar cells on paper substrates," *J. Phys. Chem. C*, vol. 118, pp. 16813–16817, 2014.
[30] C. Sprau *et al.*, "Highly efficient polymer solar cells cast from non-halogenated xylene/anisaldehyde solution," *Energy Environ. Sci.*, vol. 8, pp. 2744–2752, 2015.
[31] Q. Bao, X. Liu, S. Braun, and M. Fahlman, "Oxygen- and water-based degradation in [6,6]-phenyl-C61-butyric acid methyl ester (PCBM) films," *Adv. Energy Mater.*, vol. 4, p. 1301272, 2014.
[32] A. Guerrero *et al.*, "Oxygen doping-induced photogeneration loss in P3HT:PCBM solar cells," *Sol. Energy Mater. Sol. Cells*, vol. 100, pp. 185–191, 2012.

Victor Samuel Balderrama received the Ph.D. degree in electronic engineering, automatic, and communications from Rovira i Virgili University, Tarragona, Spain, in 2014. He is currently a Researcher with the Solid State Electronic Section, Department of Electrical Engineering, CINVESTAV-IPN, Ciudad de México, Mexico. His research interests included fabrication, characterization, and modeling of bulk heterojunction and nanostructured polymer solar cells and degradation studies. He works in collaboration with the Institute of Chemical Research of Catalonia (ICIQ), Barcelona, Spain; Rovira i Virgili University; and the Vrije University of Amsterdam, Amsterdam, the Netherlands.

Fernando Ávila-Herrera received the degree in electronics and communication engineering from National Polytechnic Institute, Ciudad de México, Mexico, in 2011. He is currently working toward the Ph.D. degree in electrical engineering with CINVESTAV-IPN, Ciudad de México.

His current research interest includes nanoscale device simulation, modeling, and device physics.

José Guadalupe Sánchez received the Industrial Chemistry Engineering degree from the National Polytechnic Institute, Ciudad de México, Mexico, in 2011. He received the Master's degree in electrical, electronic, and automatic engineering from the Rovira i Virgili University, Tarragona, Spain, in 2014, where he is currently working toward the Ph.D. degree in electronics engineering.

Josep Pallarès (S'94–A'97–M'00–SM'05) received the Ph.D. degree in physics from the Politècnica University of Catalunya, Barcelona, Spain, in 1997.

He is currently a Full Professor with the Department of Electronics Engineering, Rovira i Virgili University, Tarragona, Spain. His current research interests include characterization and modeling of advanced electron devices. He has authored and coauthored about 130 reviewed scientific publications in international journals and conference proceedings.

Osvaldo Vigil-Galán received the Ph.D. degree from University of Havana, Havana, Cuba, in 1981.

He is currently a Full Professor with the School of Physics and Mathematics, National Polytechnic Institute, Ciudad de México, Mexico. He has published more than 115 papers in international journals and has presented 122 works at international congress. His papers have been cited in more than 1024 scientific works. He is the author of eight books and five book chapters.

Lluis F. Marsal (S'94–A'97–M'01–SM'04) received the Ph.D. degree in physics from the Politècnica University of Catalunya, Barcelona, Spain, in 1997.

He is currently a Professor with the Department of Electronics Engineering, Rovira i Virgili University, Tarragona, Spain. His current research interests include nanophotonics and biosensors devices based on micro/nanoporous silicon and organic and hybrid materials for optoelectronic devices. He has authored and coauthored more than 180 reviewed scientific publications in international journals and conferences proceedings.

Prof. Marsal has been serving as a Member of the Distinguished Lecturer program of the IEEE Electron Devices Society since 2008 and as a Member of its Advisory and Technical Committees. He is Senior Member of the Optical Society of America.

Magali Estrada (M'96–SM'98) received the Ph.D. degree from NW Leningrad Institute, St. Petersburg, Russia, in 1977.

She is currently a Full Professor with CINVESTAV-IPN, Ciudad de México, Mexico. She has authored more than 210 publications, communications, and several book chapters.